**RESEARCH ARTICLE**

# Crack detection for wading-concrete structures using water irrigation and electric heating

**Jiang CHEN**[a,b,c]**, Zizhen ZENG**[c]**, Ying LUO**[c]**, Feng XIONG**[a,b,c]**, Fei CHENG**[d*]

[a] *Failure Mechanics and Engineering Disaster Prevention Key Laboratory of Sichuan Province, Sichuan University, Chengdu 610065, China*

[b] *MOE Key Laboratory of Deep Earth Science and Engineering, Sichuan University, Chengdu 610065, China*

[c] *College of Architecture and Environment, Sichuan University, Chengdu 610065, China*

[d] *College of Biomass Science and Engineering, Sichuan University, Chengdu 610065, China*

[*]*Corresponding author. E-mail: anphiacheng@163.com*

**ABSTRACT** Cracking in wading-concrete structures has a worse impact on structural safety compared with conventional concrete structures. The accurate and timely monitoring of crack development plays a significant role in the safety of wading-concrete engineering. The heat-transfer rate near a crack is related to the flow velocity of the fluid in the crack. Based on this, a novel crack-identification method for underwater concrete structures is presented. This method uses water irrigation to generate seepage at the interface of a crack; then, the heat-dissipation rate in the crack area will increase because of the convective heat-transfer effect near the crack. Crack information can be identified by monitoring the cooling law and leakage flow near cracks. The proposed mobile crack-monitoring system consists of a heating system, temperature-measurement system, and irrigation system. A series of tests was conducted on a reinforced-concrete beam using this system. The crack-discrimination index $\psi$ was defined, according to the subsection characteristics of the heat-source cooling curve. The effects of the crack width, leakage flow, and relative positions of the heat source and crack on $\psi$ were studied. The results showed that the distribution characteristics of $\psi$ along the monitoring line could accurately locate the crack, but not quantify the crack width. However, the leakage flow is sensitive to the crack width and can be used to identify it.

**KEYWORDS** structural health monitoring, underwater concrete structure, fiber Bragg grating, crack detection, temperature tracer method

## 1 Introduction

The service environment of wading-concrete structures, such as river-crossing and sea-crossing bridges, port terminals, dams, and offshore platforms, is harsh. Safety issues during construction and operation are particularly prominent. Cracks are the most common type of defects in concrete structures. In underwater concrete engineering, they not only reduce the stiffness, bearing capacity, and durability of structures, but also increase the risk of reinforcement corrosion and water leakage. The accurate and timely monitoring of the occurrence and development of cracks plays a significant role in ensuring the safety of wading-concrete engineering.

In the past, crack detection in wading-concrete engineering mainly relied on divers who visually and manually identified cracks in clear water. As technology has developed, a series of advanced non-destructive underwater-detection equipment has successively emerged, such as underwater-camera surveillance machines, ultrasonic instruments, and image sonar systems. Combining nondestructive testing methods with artificial neural networks for crack identification is a good research direction [1,2]. However, most of these detection technologies still require divers to work in an underwater environment [3].

The underwater environment is complex and changeable, and poses a great threat to the divers' safety. In addition, their short working time makes it difficult to perform long-term and large-area detection tasks. Moreover, the diving depth should generally not exceed 50 m, which makes it difficult to perform deep-water detection tasks [4]. With the development of automated control technology and artificial intelligence, various types of underwater robots have gradually replaced divers in performing various underwater operations.

There are two main types of underwater robots: cable underwater robots, which are customarily called remotely operated vehicles (ROVs) [5], and cableless underwater robots, which are customarily called autonomous underwater vehicles (AUVs) [6,7]. Researchers frequently load an enclosed underwater optical camera or sonar system onto an underwater robot to take pictures or perform sonar scanning to detect cracks in underwater structures. This method identifies cracks using deep-learning algorithms on computers to process, analyze, and understand the images [8–12]. However, this technique is time consuming and inefficient when the location of a crack is unknown in a wide detection range. Additionally, underwater robots are susceptible to interference from aquatic plants and animals. It is also difficult to perform these tasks in harsh underwater environments with rapid water flow and turbid water quality.

In practical engineering, it is more reliable to formulate crack-monitoring plans in advance and embed monitoring facilities into the concrete during the construction phase. A crack meter, mainly the resistance type, is a pre-embedded crack-monitoring instrument commonly used in civil engineering [13]. With the development of smart materials, various new materials, such as shape memory alloys [14], fiber Bragg gratings (FBG) [15], and piezoelectric ceramics [16], have been extensively studied in the crack-sensor manufacturing field. These types of embedded sensors are generally only placed in key positions, which are prone to misjudgment. In addition, pre-embedded sensors cannot be replaced once damaged and fail to meet the long-term monitoring requirements of engineering structures. Therefore, it is imperative to develop a new monitoring method to solve the technical difficulties of crack monitoring in wading concrete.

Temperature is an important physical quantity in daily production and life. It exhibits a coupling effect with many physical quantities. Therefore, various physical quantities can be indirectly identified by measuring the temperature-change law [17]. This is the so-called temperature-tracer method. At present, this method has been studied and applied extensively in many engineering-monitoring fields, such as tunnel fires [18], oil-pipeline leakage [19], soil water content [20–22], rockfill dam seepage [23–30], pile-foundation integrity [31], scouring around submarine pipelines [32], voids in concrete-face rockfill dams [33], and debris-flow warnings [34]. Chen et al. [35] proposed a temperature-tracer detection method for cracks in underwater concrete structures with a series of embedded porous casing tubes. When the structure cracks, the moisture content of the porous casing tube increases in the cracked position, resulting in an increase in the thermal conductivity of the cracked casing tube. The crack position can then be identified, according to the abnormal cooling law. To improve the monitoring effects, Zhu et al. [36] replaced the porous casings with hollow casings.

However, these two methods cannot quantify the width of cracks in still water, and the location accuracy of the cracks depends on the casing length. Therefore, this study presents a novel crack-monitoring method for wading-concrete engineering using an active irrigation-heating method. The feasibility of this method was verified through a series of experiments.

## 2   Monitoring system and principle

The basic approach to crack monitoring based on thermal effects is to change the thermodynamic parameters or heat-transfer boundary conditions of the medium around the cracks. Based on this principle, our proposed crack-monitoring system consists of a heating system, temperature-measurement system, and irrigation system (shown in Fig. 1). The monitoring tube and irrigation pipe were pre-embedded in the structure. FBG-sensing technology was used for temperature measurement, and has the advantage of multiple points connected in series. The irrigation pipe was fabricated with brittle materials to ensure cracks within the monitored structure.

The position of each sensing-heating element can be changed by dragging the sensing-heating integrated circuit. Therefore, the spatial resolution can be improved through multiple measurements. Moreover, the sensing-heating elements can be removed from the monitoring tube for repair or replacement to satisfy the long-term monitoring requirements of wading-concrete engineering.

Two different methods can be used to determine whether cracks occur, using this monitoring system. In the first situation, that is, no preset water in the irrigation pipe, as shown in Fig. 1(a), water seeps into the irrigation pipe from cracks when they form. Therefore, if water is found in the irrigation pipe (this can be measured by the water gauge), it can be concluded that cracks have formed in the monitoring tube. In the second situation, with a water-filled irrigation pipe, as shown in Fig. 1(b), the water in the irrigation pipe seeps out through the cracks, owing to the pressure difference when cracks occur. Therefore, the water level in the irrigation pipe drops. This indicates that cracks have formed in the monitoring line.
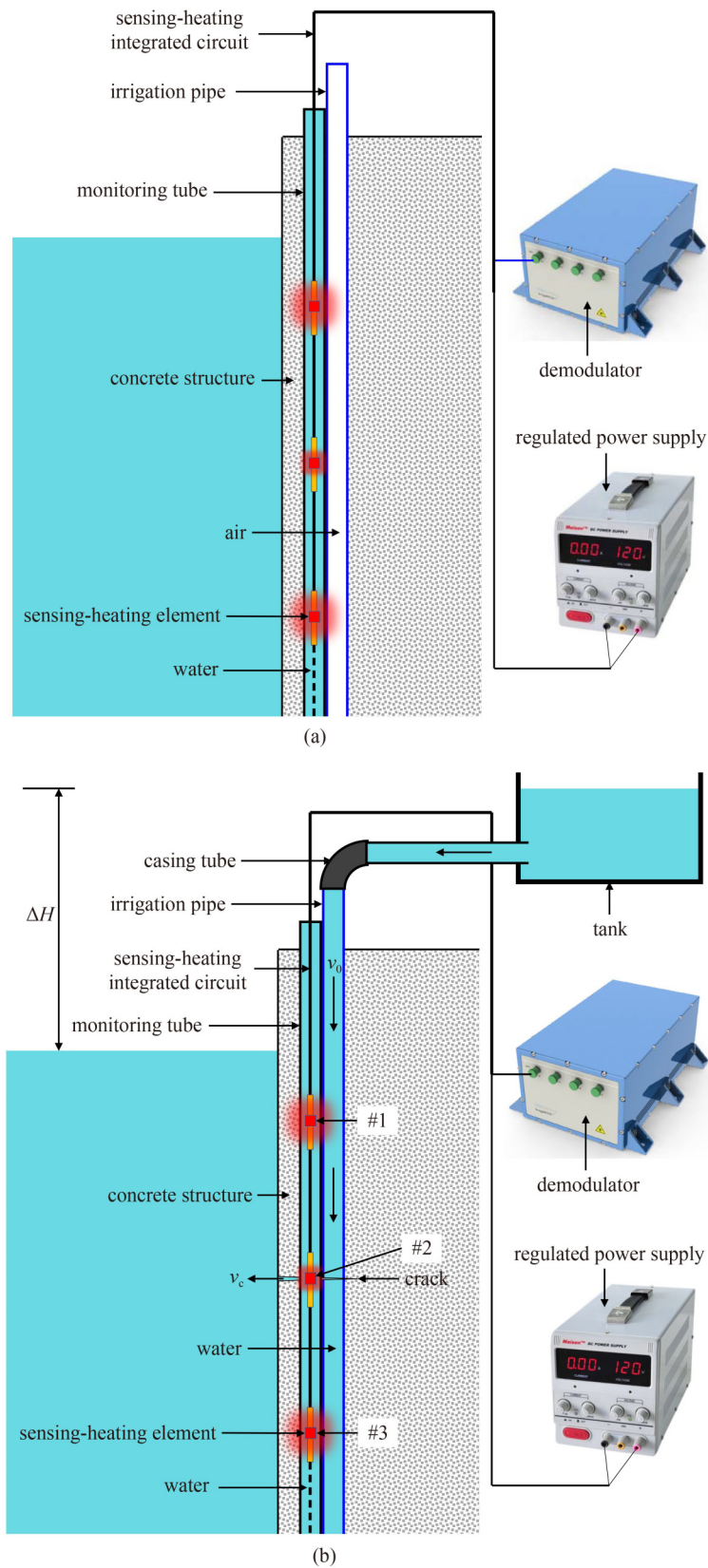
To further determine the location and width of the

**Fig. 1**  Scheme of a crack-monitoring system for underwater concrete structures: (a) uncracked; (b) cracked.

crack, the irrigation pipe is connected to a constant-level water tank using a casing tube, as shown in Fig. 1(b). A constant-level water tank can be implemented as shown in Fig. 2.

Owing to the difference in water pressure, the water in the irrigation pipe flows into the external environment through the crack, producing convection at the crack interface. A schematic of the thermal effect near a crack is shown in Fig. 3. It is assumed that the width of the crack is $w$, the distance between the crack and the sensing-heating element is $d_c$, the flow velocity in the irrigation pipe is $v_0$, and the flow velocity in the crack is $v_c$. $v_0$ can be determined from the leakage flow $q_w$ and the cross-sectional area $A_f$ of the irrigation pipe, using the following equation:

$$v_0 = \frac{q_w}{A_f}. \tag{1}$$

When the sensing-heating element is located under the crack (such as measuring point #3 in Fig. 1(b)), the nearby water in the irrigation pipe is still. The heat released by this sensing-heating element is transferred outward mainly through heat conduction. Its heat-flux density is related to the thermal conductivity and temperature gradient of the surrounding medium:

$$\{q_h\} = \{L\}^T [D] \{L\} T, \tag{2}$$

$$\{L\} = \left\{ \frac{\partial}{\partial x}, \frac{\partial}{\partial y}, \frac{\partial}{\partial z} \right\}^T, \tag{3}$$

$$[D] = \begin{bmatrix} K_x & 0 & 0 \\ 0 & K_y & 0 \\ 0 & 0 & K_z \end{bmatrix}, \tag{4}$$

where $\{q_h\}$ is the heat-flux vector generated by heat conduction; $[D]$ is the conductivity matrix; $T$ is the temperature; $\{L\}$ is the vector operator; and $K_x$, $K_y$, and $K_z$ are the thermal conductivities of the medium in the $x$, $y$, and $z$ directions, respectively.

When the sensing-heating element is above the crack (such as measuring point #1 in Fig. 1(b)), the water around it in the irrigation pipe flows. Its heat-transfer mode includes both heat conduction and convection. The heat-flux density generated by the flowing water can be expressed as

$$\{q_c\} = \rho_w c_w T \{v\}^T \{L\}, \tag{5}$$

$$\{v\} = \{v_x, v_y, v_z\}^T, \tag{6}$$

where $\{q_c\}$ is the heat-flux vector generated by water flow, $\rho_w$ is the density of water, $c_w$ is the specific heat of water, $\{v\}$ is the velocity vector of water, and $v_x$, $v_y$, and $v_z$ are the velocities of water in the $x$, $y$, and $z$ directions, respectively.

When the sensing-heating element is close to the crack (such as measuring point #2 in Fig. 1(b)), the water flow in the crack will have a convective effect on the sensing-
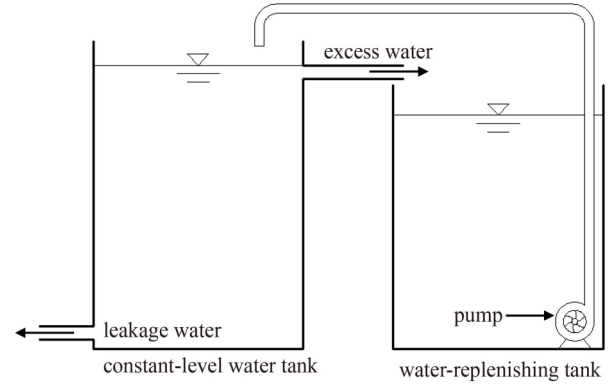


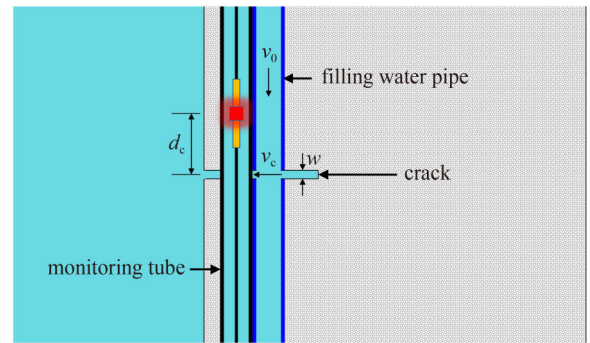**Fig. 2** Scheme of the implementation of a constant-level water tank.



**Fig. 3** Sketch of the thermal effect near a crack.

heating element. Because the crack is narrow, $v_c$ is much larger than $v_0$, and the contact area between the irrigation pipe and the monitoring tube is small; therefore, the convective heat-transfer effect near measuring point #2 is stronger than that at measuring point #1.

For large wading-concrete engineering, the monitoring line may be very long. Unfortunately, the number of sensing-heating elements that can be connected in series on each integrated circuit is limited; generally, no more than 20. With a separated sensing-heating integrated circuit and monitoring tube, the measuring points on the entire monitoring line can be fully covered by dragging the sensing-heating integrated circuit to change the position of the sensing-heating elements. In summary, when mobile distributed monitoring is conducted along the entire monitoring line, the crack locations can be determined according to the difference in cooling rate, and the crack width can be determined using the relationship between the leakage flow, crack width, and water head.

## 3 Experiment

### 3.1 Test specimen

The reinforced-concrete beam shown in Fig. 4 was

designed as a test specimen. Two rebars with a 6-mm diameter and 110-mm spacing were pre-embedded 30 mm from the bottom of the specimen. A ceramic pipe with a 14-mm inner diameter and 18-mm outer diameter was used as the filling water pipe. A polyethylene of raised temperature resistance (PE-RT) tube with a 16-mm inner diameter and 20-mm outer diameter was used as the monitoring tube. Both were pre-embedded in the specimen at their corresponding positions, as shown in Fig. 4. The bottoms of both the monitoring tube and the filling water pipe (right side of Fig. 4) were sealed with a hot-melt adhesive.

## 3.2    Test devices

First, the specimen was cracked in the middle through three point-bending tests, and the crack width was observed using a crack microscope. The specimen was then placed in an upright position and immersed in a bucket. A hole was drilled in the side of the bucket 50 cm from the bottom. Excess water overflows from the hole during irrigation to maintain the water level in the bucket. A flexible casing tube was used to connect the leakage pipe to the water tank and irrigation pipe pre-embedded in the specimen, and the leakage pipe was equipped with a valve to control the flow rate. A photograph of the test site is shown in Fig. 5.

An FBG demodulator with a 1528–1568-nm wavelength range was used in the test. Its wavelength resolution and measurement accuracy are 0.1 and ± 0.5 pm, respectively. The sampling frequency can reach 1000 Hz, and the dynamic range is greater than 25 dB. A sectional view of the sensing-heating element used in the test is shown in Fig. 6.

## 3.3    Test procedure

The cooling laws of the heat source at each measuring point, shown in Fig. 7, were tested under the combined working conditions with different crack widths and leakage flows. The test steps were as follows.

1) The specimen was immersed in the bucket for more than 24 h. The sensing-heating element was inserted into the monitoring tube, and its position was adjusted by dragging the armored optical cable.

2) The sampling frequency of the demodulator and the heating voltage of the regulated power supply were adjusted to 1 Hz and 12 V, respectively.
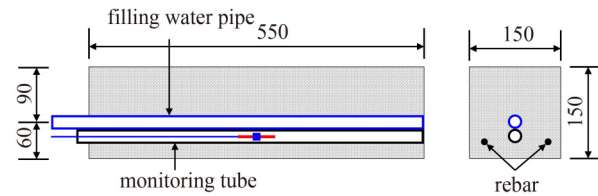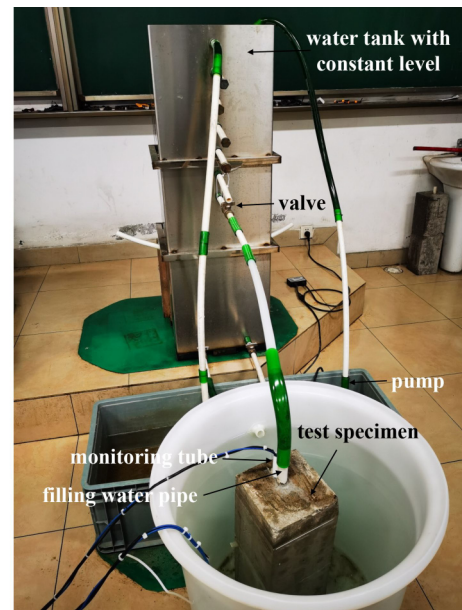


**Fig. 4**    Sketch of test specimen.



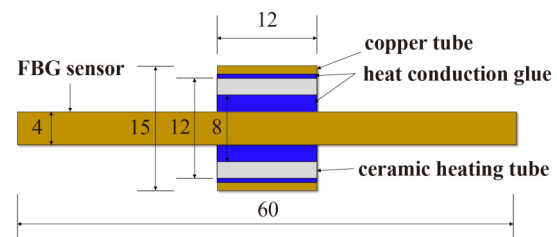**Fig. 5**    Test site in still water.



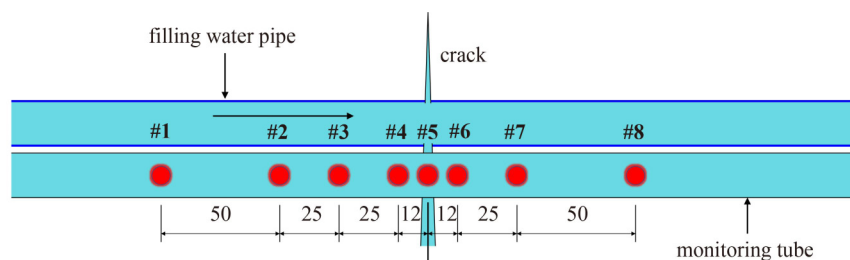**Fig. 6**    Sectional view of sensing-heating element.



**Fig. 7**    Layout of measuring points.

3) The valve was adjusted to fill the irrigation pipe. The leakage flow $q_w$ was measured from the immersed specimen using a measuring cylinder.

4) When $q_w$ was stable, the wavelength of the FBG sensor was tested under the ambient temperature, and the test duration was at least 1 min. The average value of the wavelength tested within 1 min was used as the wavelength $\lambda_\theta$ corresponding to the ambient temperature.

5) The regulated power supply was turned on to start heating, and turned off after 3 min. The wavelength was tested during the heating and cooling stages until it was stable.

6) The position of the sensing-heating element was adjusted and step 5) was repeated for the other measuring points.

# 4　Results and analysis

The heating laws of the sensing-heating element at each measuring point were basically the same when the heating time and voltage were both constant. Therefore, it is difficult to identify crack information or leakage through heating curves using this monitoring system [27]. Chen et al. [30] presented a method for identifying leakage using cooling curves and achieved good results. In this study, the cooling law of the sensing-heating element was used to identify cracks.

First, a dimensionless parameter $\Gamma$ that reflects the relative cooling degree of the sensing-heating element is defined as follows:

$$\Gamma = \frac{T - T_\theta}{T_0 - T_\theta},\qquad(7)$$

where $T_0$ is the temperature of the measurement point at the initial time during the cooling stage, $T_\theta$ is the ambient temperature, and $T$ is the temperature of the measurement point at any moment during the cooling stage. Because the central wavelength of the FBG temperature sensor is linear with the temperature, $\Gamma$ can also be expressed as

$$\Gamma = \frac{\lambda - \lambda_\theta}{\lambda_0 - \lambda_\theta},\qquad(8)$$

where $\lambda$, $\lambda_\theta$, and $\lambda_0$ are the center wavelengths of the FBG temperature sensor at temperatures $T$, $T_\theta$, and $T_0$, respectively.

## 4.1　Cooling law of a sensing-heating element in still water

Heating and cooling tests were performed for different crack widths and leakage flows in still water. As an example, the time–history curves of $\Gamma$ at each measuring point, when $w = 0.6$ mm and $q_w = 100$ mL·min$^{-1}$, were plotted in semilogarithmic coordinate axes, as shown in Fig. 8. This shows that lg$\Gamma$ exhibits linear characteristics from 150 to 600 s. The slopes in this period can better

reflect the relative position between the measuring point and crack. In other words, the absolute value of the slope increases with a decrease in the distance between the measuring point and crack. Therefore, the slope of the curve from 150 to 600 s was defined as the crack-discrimination index $\psi$ in the subsequent analysis, and can be calculated using the least-squares method. The variation law of the slope under other working conditions was similar.

## 4.2　Effect of water environment on the cooling law of the sensing-heating element

In practical engineering, the environment around an underwater concrete structure is complex and changeable. Moreover, it may not be in still water, but in a flow field. If the external flow field influences the cooling law of the sensing-heating element in the structure, the wider the crack and the shorter the distance between the measuring point and the crack, the more significant the effect is. Therefore, we tested a specimen with the maximum test crack width ($w = 1.6$ mm) in flowing water. To build a lotic environment in the bucket shown in Fig. 5, a pump with a 90-W power and 6.5-m lift was placed in the bucket to circulate the water, as shown in Fig. 9.
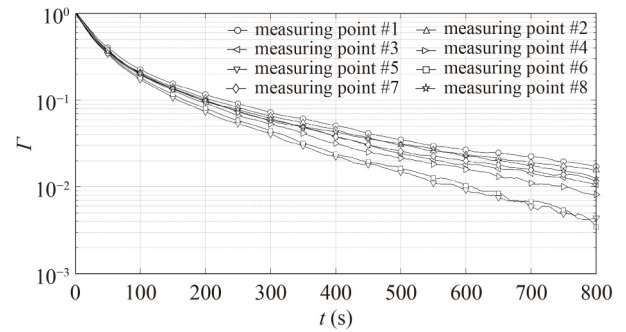


**Fig. 8**　Semilogarithmic graph of time–history curves of $\Gamma$.



**Fig. 9**　Test site in flowing water.

A comparison of the time–history curves of $\lg\Gamma$ at measuring point #5 in both still and flowing water is shown in Fig. 10. The curves are essentially the same, indicating that the external flow field has little effect on the cooling law of the sensing-heating element. This is because the sensing-heating element used in this study can be regarded as a point heat source (PHS) with low heat and a small influence range. The heat-transfer law of the PHS is only affected by a small range near it.

### 4.3 Crack location

Using the above method, the values of $\psi$ corresponding to each measuring point under each working condition were calculated, and their distribution characteristics are shown in Fig. 11. The calculated value of $\psi$ in the uncracked

state is $-1.606 \times 10^{-3}$. The dotted line ($\psi = -1.606 \times 10^{-3}$) shown in Fig. 11 was taken as the baseline. The following can be observed from Fig. 11.
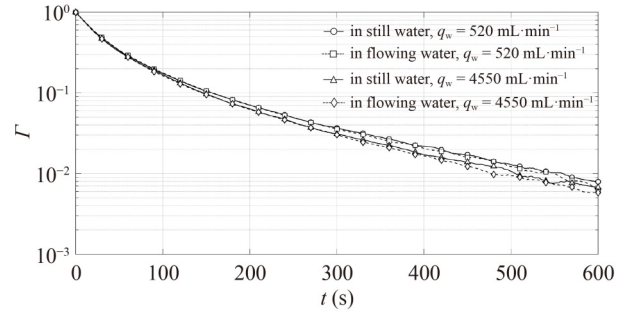


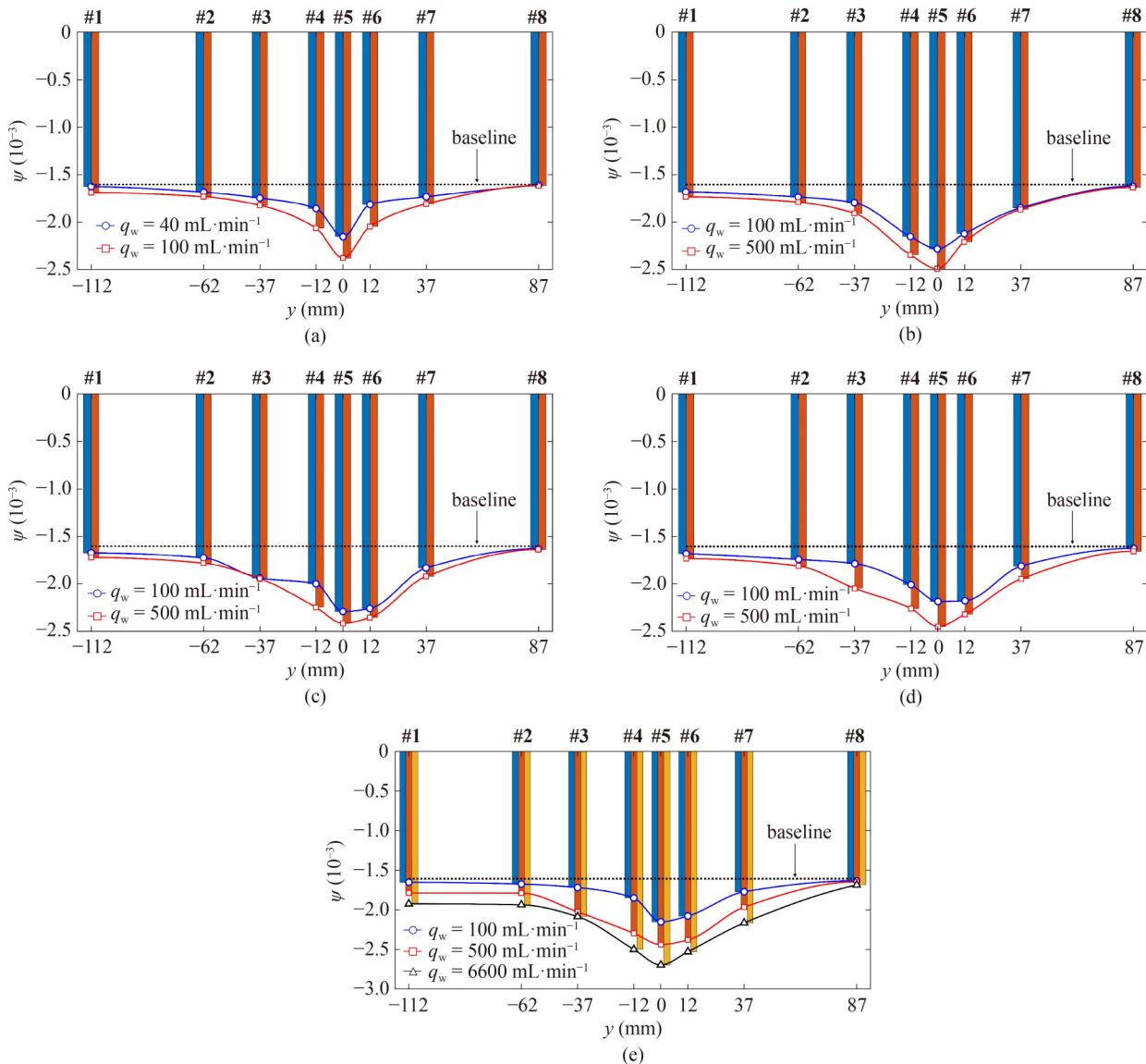**Fig. 10**  Comparison of the time–history curves of $\lg\Gamma$ in still water and flowing water.



**Fig. 11**  Distribution of $\psi$ with different crack widths and leakage flows: (a) $w = 0.2$ mm; (b) $w = 0.4$ mm; (c) $w = 0.6$ mm; (d) $w = 1.0$ mm; (e) $w = 1.6$ mm.

1) The shorter the distance between the measuring point and crack, the larger the absolute value of $\psi$; therefore, the distribution characteristics of $\psi$ can accurately locate the crack.

2) When the crack width is constant, the flow velocity in the crack increases with an increase in the leakage flow, and the absolute value of $\psi$ increases accordingly.

3) The flow velocity in the irrigation pipe under the crack is close to zero; therefore, the cooling law of the measuring points located under the crack (measuring points #6–#8) is mainly affected by $v_c$. The greater the distance between the measuring point and crack, the less the cooling law of the sensing-heating element is affected. For example, the value of $\psi$ at measuring point #8 is basically the same as that in the uncracked state, indicating that the cooling law of measuring point #8 is nearly unaffected by $v_c$.

4) The flow velocity in the irrigation pipe over the crack was proportional to the leakage flow, and the cooling law of the measuring points located over the crack (measuring points #1–#4) was affected by both $v_0$ and $v_c$. Therefore, compared with measuring point #8, although measuring point #1 is farther away from the crack, the absolute value of $\psi$ at measuring point #1 is greater and tends to increase with the increase in leakage flow.

To verify the effectiveness of $\psi$ for locating multiple cracks, another specimen was fabricated with the same cross-section as that in Fig. 4 and a 100-cm length. Two cracks with 0.3-mm and 1.0-mm widths, 68 and 33 cm above the bottom, respectively, were created in this specimen. The distribution of $\psi$ along the height of the specimen, when the spacing between the measuring points was 5 cm, is shown in Fig. 12. This shows that the distribution characteristics of $\psi$ can locate both cracks
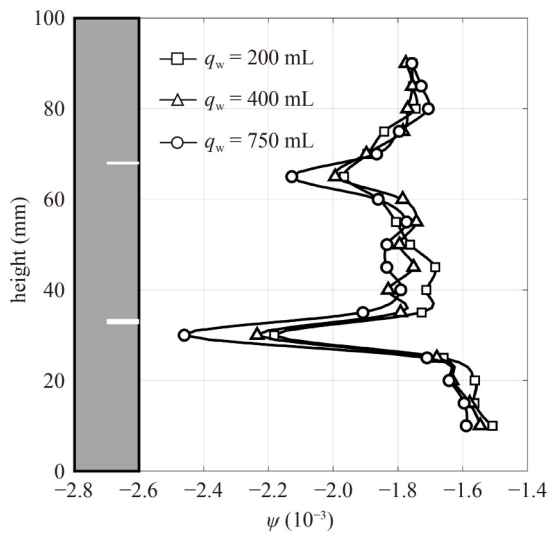
well and qualitatively reveal the crack width. The greater the leakage flow, the better the identification effect.

### 4.4 Effect of leakage flow on monitoring results

When the crack width is constant, the convective heat-transfer effect and cooling rate of the sensing-heating element will increase with an increase in the leakage flow. The relationship between $\psi$ and $q_w$ at measuring point #5 is plotted in semilogarithmic coordinate axes, under combined working conditions with different crack widths and leakage flows, as shown in Fig. 13. This shows that the absolute value of $\psi$ tends to increase with an increase in leakage flow; however, the increasing magnitude gradually decelerates. The results indicate that the greater the leakage flow, the greater the difference in $\psi$ between the cracked and uncracked parts. Therefore, the monitoring effect can be improved by increasing the leakage flow.

### 4.5 Crack-width identification

As shown in Fig. 3, $\psi$ is related to $w$, $d_c$, and $q_w$. Owing to the spatial-resolution limitation in practical applications, it is difficult to accurately determine $d_c$. The relationship between $\psi$ and $w$ for measuring point #5 ($d_c = 0$) when $q_w$ is constant is shown in Fig. 14. This shows that $\psi$ changes slightly with an increase in the crack width when $d_c$ is constant. This is because the convective effect
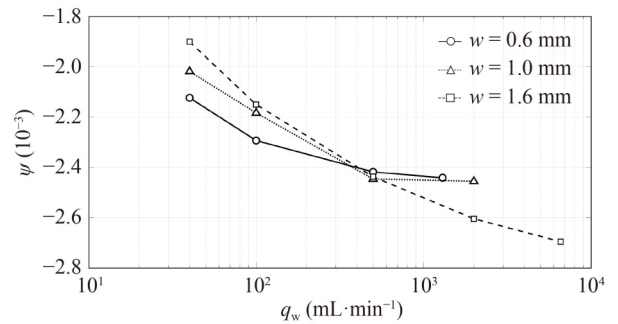
**Fig. 13** Relationship between $q_w$ and $\psi$ for measuring point #5.

**Fig. 12** Distribution of $\psi$ under different crack widths and leakage flows.
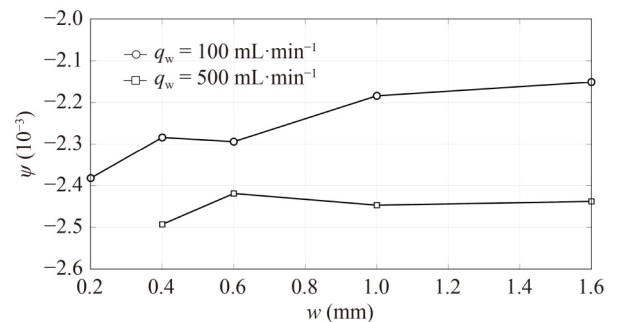
**Fig. 14** Relationship between $\psi$ and $w$ for measuring point #5.

is related to both $v_c$ and the convective surface. When the leakage flow is constant, $v_c$ decreases with an increase in the crack width, but the convective surface increases. Under the integrated effects of $v_c$ and the convective surface, it is difficult to follow the variation characteristics of $\psi$ with the crack width. Furthermore, a gap exists between the sensing-heating element and the inner wall of the monitoring tube, and the relative position of the sensing-heating element in the monitoring tube has a slight influence on $\psi$. For these reasons, it is difficult to quantify the crack width with $\psi$.

As the crack width increased, the permeability at the crack part and the leakage flow increased when the water-head difference was constant ($\Delta H$, the difference between the water level of the water tank and bucket shown in Fig. 5). To obtain the relationships between $q_w$ and $w$ with various water-head differences, four specimens were tested, and the calibration results are shown in Fig. 15. The fitting relationship between them within the tested range of crack widths is given by Eq. (9). This shows that the relationship between the leakage flow and crack width is a power function. In summary, $\psi$ can be used to locate cracks, and leakage flow can be used to quantify the degree of cracking, based on their calibration relationship.

$$\begin{cases} q_w = 1595.698w^{2.316}, \Delta H = 70 \, \text{cm} \, (R^2 = 0.98655), \\ q_w = 2161.253w^{2.265}, \Delta H = 130 \, \text{cm} \, (R^2 = 0.98907), \\ q_w = 2659.015w^{2.185}, \Delta H = 180 \, \text{cm} \, (R^2 = 0.99169). \end{cases} \quad (9)$$

When there are multiple cracks on the same monitoring line, it is difficult to determine the leakage flow at each crack. Only the overall cracking degree of the monitoring line can be obtained. The width of each crack cannot be identified. We will further study the effect of the axial velocity ($v_0$) in the irrigation pipe on the cooling law of the heat source in the monitoring tube and then determine a method to identify $v_0$. In this manner, we can determine the leakage flow at each crack, according to the change in the axial velocity in the irrigation pipe, to determine the width of each crack. To improve the sensitivity of the effect of $v_0$ on the cooling law of the heat source, the
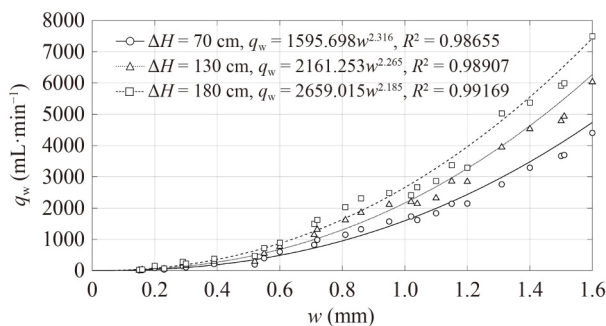
**Fig. 15** Relationship between $q_w$ and $w$.

configuration of the monitoring tube and irrigation pipe must be further optimized.

## 5  Conclusions

The fluid flow in a crack produces a convective effect at the crack interface, and the permeability of the cracked part is related to the crack width. Based on this thermodynamic phenomenon, a crack-monitoring method for wading-concrete engineering with water irrigation and electric heating was presented, and a mobile distributed monitoring system was designed. A series of tests was conducted on a reinforced-concrete beam to investigate the effects of the crack width, leakage flow, and relative positions of the measuring points and crack on the cooling law of the sensing-heating element. The following conclusions were drawn.

1) Over a certain period of time (from 150 to 600 s in this study), the time–history curve of $\lg \Gamma$ has linear characteristics, and the slope $\psi$ of this linear segment can be used as a crack-discrimination index.

2) The absolute value of $\psi$ will increase with a decrease in the distance between the measuring point and the crack; hence, the crack can be accurately located according to the distribution of $\psi$.

3) When the crack width is constant, the absolute value of $\psi$ shows an increasing trend with an increase in leakage flow. The monitoring effect can be improved by increasing the leakage flow.

4) Many factors influence $\psi$; hence, it is difficult to quantitatively identify the crack width with $\psi$. The leakage flow is sensitive to the crack width, which has a power-function relationship with the crack.

## References

1. Saleem M, Gutierrez H. Using artificial neural network and non-destructive test for crack detection in concrete surrounding the embedded steel reinforcement. Structural Concrete, 2021, 22(5): 2849−2867

2. Hosoda A, Adnan A, Saleem M, Yoshida Y. Improvement of artificial neural network model for thermal crack width in RC abutments using actual construction data. Proceedings of Japanese Concrete Institute—JCI Annual Proceedings, 2022, 44(1): 970−975

3. Huang C, Li F, Zhou R. Inspection and treatment of underwater crack of upstream surface of first-stage project of Danjiangkou Dam. Yangze River, 2015, 46(6): 41−44 (in Chinese)

4. Bei Q R. Detecting technologies for underwater projects and its application. Large Dam and Safety, 2004, 1: 37−39 (in Chinese)

5.  Chowdhury T, Sathianarayanan D, Dharani G, Ramadass G A. Failure analysis of fasteners in a remotely operated vehicle (ROV) system. Journal of Failure Analysis and Prevention, 2015, 15(6): 915−923

6.  Jacobi M. Autonomous inspection of underwater structures. Robotics and Autonomous Systems, 2015, 67: 80−86

7.  Wang X, Zhang G, Sun Y, Cao J, Wan L, Sheng M, Liu Y. AUV near-wall-following control based on adaptive disturbance observer. Ocean Engineering, 2019, 190: 106429

8.  Shi P, Fan X, Ni J, Wang G. A detection and classification approach for underwater dam cracks. Structural Health Monitoring, 2016, 15(5): 541−554

9.  Savino P, Tondolo F. Automated classification of civil structure defects based on convolutional neural network. Frontiers of Structural and Civil Engineering, 2021, 15(2): 305−317

10.  Cha Y J, Choi W, Büyüköztürk O. Deep learning-based crack damage detection using convolutional neural networks. Computer-Aided Civil and Infrastructure Engineering, 2017, 32(5): 361−378

11.  Cha Y J, Choi W, Suh G, Mahmoudkhani S, Büyüköztürk O. Autonomous structural visual inspection using region-based deep learning for detecting multiple damage types. Computer-Aided Civil and Infrastructure Engineering, 2018, 33(9): 731−747

12.  Kang D H, Cha Y J. Efficient attention-based deep encoder and decoder for automatic crack segmentation. Structural Health Monitoring, 2022, 21(5): 2190−2205

13.  Chakraborty J, Katunin A, Klikowicz P, Salamak M. Early crack detection of reinforced concrete structure using embedded sensors. Sensors (Basel), 2019, 19(18): 1−22

14.  Zhang Y, Li J, Wang Q, Liu B. Mechanism and experimental study on crack monitoring and repair of shape memory alloy intelligent concrete. Acta Mechanica Solida Sinica, 2020, 41(2): 170−181 (in Chinese)

15.  Tian C B, Wang J, Zhang F, Sui Q M, Sun B, Wang Z F, Li Y J. Study of fiber bragg grating sensor for monitoring of concrete cracks in bridge steel tube. Instrument Technique and Sensor, 2017, 9: 20−23 (in Chinese)

16.  Jiang T, Hong Y, Zheng J, Wang L, Gu H. Crack detection of FRP-reinforced concrete beam using embedded piezoceramic smart aggregates. Sensors (Basel), 2019, 19(9): 1−20

17.  He F, Chen J, Li C, Xiong F. Temperature tracer method in structural health monitoring: A review. Measurement, 2022, 200: 111608

18.  Aralt T T, Nilsen A R. Automatic fire detection in road traffic tunnels. Tunnelling and Underground Space Technology, 2009, 24(1): 75−83

19.  Madabhushi S S C, Elshafie M, Haigh S K. Accuracy of distributed optical fiber temperature sensing for use in leak detection of subsea pipelines. Journal of Pipeline System Engineering and Practice, 2015, 6(2): 04014014

20.  Cao D F, Shi B, Zhu H H, Inyang H I, Wei G Q, Duan C Z. A soil moisture estimation method using actively heated fiber Bragg grating sensors. Engineering Geology, 2018, 242: 142−149

21.  de Morais Franca M B, Morais F J O, Carvalhaes-Dias P, Duarte L C, Siqueira Dias J A. A multiprobe heat pulse sensor for soil moisture measurement based on PCB technology. IEEE Transactions on Instrumentation and Measurement, 2019, 68(2): 606−613

22.  He F, Zhang C, Chen J, Xiong F. Study on the mobile PHS method for soil moisture monitoring based on thermal effect. IEEE Sensors Journal, 2021, 21(13): 15209−15217

23.  Khan A A, Vrabie V, Beck Y L, Mars J I, D'Urso G. Monitoring and early detection of internal erosion: Distributed sensing and processing. Structural Health Monitoring, 2014, 13(5): 562−576

24.  Vogt T, Schneider P, Hahn-Woernle L, Cirpka O A. Estimation of seepage rates in a losing stream by means of fiber-optic high-resolution vertical temperature profiling. Journal of Hydrology (Amsterdam), 2010, 380(1−2): 154−164

25.  Su H, Li H, Kang Y, Wen Z. Experimental study on distributed optical fiber-based approach monitoring saturation line in levee engineering. Optics & Laser Technology, 2018, 99: 19−29

26.  Cote A, Carrier B, Leduc J, Noël P, Gervais R. Water leakage detection using optical fiber at the Peribonka dam. In: Proceedings of the 7th International Symposium on Field Measurments in Geomechanics. Boston, MA: ASCE, 2007, 1−12

27.  Chen J, Cheng F, Xiong F, Ge Q, Zhang S. An experimental study: Fiber Bragg grating-hydrothermal cycling integration system for seepage monitoring of rockfill dams. Structural Health Monitoring, 2017, 16(1): 50−61

28.  Chen J, Zheng J, Xiong F, Ge Q, Yan Q, Cheng F. Experimental investigation of leak detection using mobile distributed monitoring system. Smart Materials and Structures, 2018, 27(1): 015025

29.  Chen J, Xiong F, Zheng J, Ge Q, Cheng F. The influence of infiltration angle on the identification effect of seepage with linear heat source method. Measurement, 2019, 148: 106974

30.  Chen J, Fang X, Cheng F, Ge Q, Xiong F. Sensitivity analysis and seepage/leakage monitoring using point heat source. Geotechnique, 2021, 71(10): 911−924

31.  Liu Y, Xiao H, Huang S, Wu W, Chen Z. Research on the layout of optical fibers applied for determining the integrity of cast-*in-situ* piles. Optical Fiber Technology, 2018, 45: 173−181

32.  Zhao X, Ba Q, Li L, Gong P, Ou J. A three-index estimator based on active thermometry and a novel monitoring system of scour under submarine pipelines. Sensors and Actuators. A, Physical, 2012, 183: 115−122

33.  Chen J, Song Y, Xiong F, Ai T. A thermal effects-based method for void detection in concrete face rockfill dams. IEEE Transactions on Instrumentation and Measurement, 2022, 71: 1001307

34.  Chen J, Luo Y, Xiong J, Zhang S J, Xia M Y, Yang H J, Ge Q. A thermal-effect-based monitoring method for debris flow warning. Geomorphology, 2022, 400: 108097

35.  Chen J, Xiong F, Zhu Y, Yan H. A crack detection method for underwater concrete structures using sensing-heating system with porous casing. Measurement, 2021, 168: 108332

36.  Zhu Y, Chen J, Zhang Y, Xiong F, He F, Fang X. Temperature tracer method for crack detection in underwater concrete structures. Structural Control and Health Monitoring, 2020, 27(9): e2595